ACS PHYSICAL CHEMISTRY Au
AN OPEN ACCESS JOURNAL OF THE AMERICAN CHEMICAL SOCIETY

pubs.acs.org/physchemau

Article

Development of Two-Dimensional Electronic-Vibrational Sum Frequency Generation (2D-EVSFG) for Vibronic and Solvent Couplings of Molecules at Interfaces and Surfaces

Zhi-Chao Huang-Fu, Yuqin Qian, Gang-Hua Deng, Tong Zhang, Sydney Schmidt, Jesse Brown, and Yi Rao*

Cite This: *ACS Phys. Chem Au* 2023, 3, 374–385

Read Online

ACCESS | Metrics & More | Article Recommendations | Supporting Information

ABSTRACT: Many photoinduced excited states' relaxation processes and chemical reactions occur at interfaces and surfaces, including charge transfer, energy transfer, proton transfer, proton-coupled electron transfer, configurational dynamics, conical intersections, etc. Of them, interactions of electronic and vibrational motions, namely, vibronic couplings, are the main determining factors for the relaxation processes or reaction pathways. However, time-resolved electronic-vibrational spectroscopy for interfaces and surfaces is lacking. Here we develop interface/surface-specific two-dimensional electronic-vibrational sum frequency generation spectroscopy (2D-EVSFG) for time-dependent vibronic coupling of excited states at interfaces and surfaces. We further demonstrate the fourth-order technique by investigating vibronic coupling, solvent correlation, and time evolution of the coupling for photoexcited interface-active molecules, crystal violet (CV), at the air/water interface as an example. The two vibronic absorption peaks for CV molecules at the interface from the 2D-EVSFG experiments were found to be more prominent than their counterparts in bulk from 2D-EV. Quantitative analysis of the vibronic peaks in 2D-EVSFG suggested that a non-Condon process participates in the photoexcitation of CV at the interface. We further reveal vibrational solvent coupling for the zeroth level on the electronic state with respect to that on the ground state, which is directly related to the magnitude of its change in solvent reorganization energy. The change in the solvent reorganization energy at the interface is much smaller than that in bulk methanol. Time-dependent center line slopes (CLSs) of 2D-EVSFG also showed that kinetic behaviors of CV at the air/water interface are significantly different from those in bulk methanol. Our ultrafast 2D-EVSFG experiments not only offer vibrational information on both excited states and the ground state as compared with the traditional doubly resonant sum frequency generation and electronic-vibrational coupling but also provide vibronic coupling, dynamical solvent effects, and time evolution of vibronic coupling at interfaces.

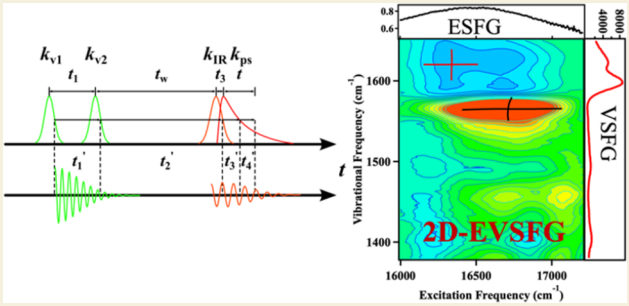

KEYWORDS: *vibronic coupling, two-dimensional electronic-vibrational sum frequency generation, double-resonance sum frequency generation, ultrafast interfacial processes, non-Condon process, center line slopes*

INTRODUCTION

Interfaces and surfaces play vital roles in almost all natural and artificial phenomena such as solar energy conversion, environmental issues, artificial photosynthesis, etc.[1−7] Understanding photoinduced dynamic processes and chemical reactions at interfaces and surfaces is crucial for revealing the nature of natural and artificial phenomena. Upon photoillumination, many photoinduced physical processes and chemical reactions subsequently occur at interfaces and surfaces. These interfacial physics and chemistry are intimately correlated with fundamental steps such as electron or hole transfer, proton transfer, proton-coupled electron/hole transfer, configurational dynamics, conical intersections, and energy transfer.[8−10] The reaction rates for such steps are dictated by both electronic and nucleic motions. Electronic-nucleic interactions in these perturbed electronic states are key to photoinduced chemistry with ultrafast time resolution. However, dynamical interactions of electronic and nucleic motions at interfaces and surfaces have not been exploited.

It is worth mentioning that static interactions of electronic and nucleic motions at interfaces and surfaces were demonstrated more over decades ago.[11−14] Such a technique is frequency-domain doubly resonant sum frequency generation

Received: March 9, 2023
Revised: April 10, 2023
Accepted: April 11, 2023
Published: April 25, 2023

https://doi.org/10.1021/acsphyschemau.3c00011
ACS Phys. Chem Au 2023, 3, 374–385

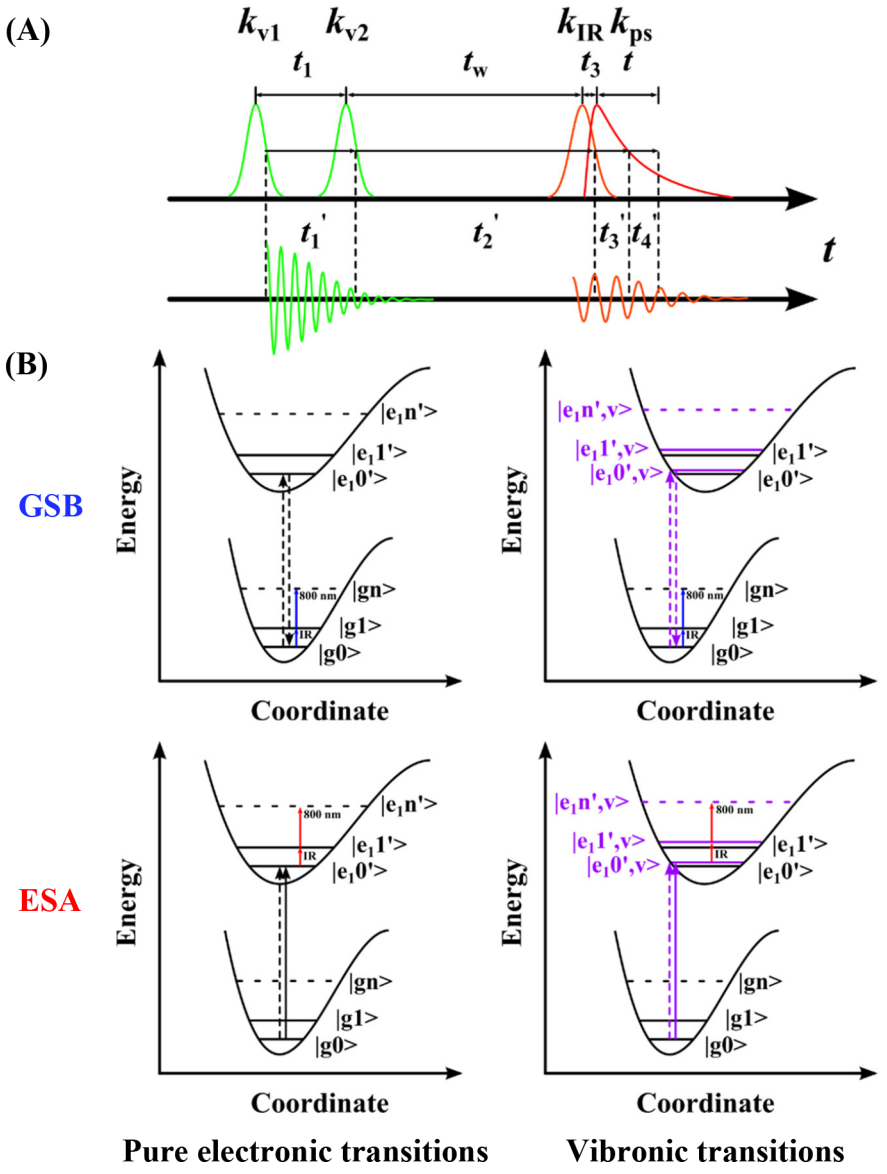

Figure 1. (A) Physical time delays of the four laser pulses for 2D-EVSFG (upper). The coherence time delay, t_1, is defined as the one between k_{V1} and k_{V2}. The waiting time delay, t_w, is defined as the delay between the pump pair and the mid-IR. t_3 is between the IR and the ps 800 nm, and the detection time t is between the ps and signal. The response time delays between four electric field-matter interactions are specified by t_1', t_2', t_3', and t_4'. (B) Energy diagram of a pure electronic transition (left) and a vibronic transition (right) when the pump pair interacts with molecules. |g0>, |g1>, and |gn> denote vibrational states of 0, 1, and manifold n in the ground state. $|e_10'>$, $|e_11'>$, and $|e_1n'>$ represent manifold vibrational states of 0′, 1′, and manifold n′ in the pure electronic excited state. $|e_10',\nu>$, $|e_11',\nu>$, and $|e_1n',\nu>$ denote vibrational states of 0′, 1′, and manifold n′ in a vibronic excited state that is coupled with excitation of a low frequency, ν. Blue and red arrows indicate the GSB and ESA 2D-EVSFG signals.

(DR-SFG), which is generated by mixing a visible beam and an IR beam. The IR beam is varied to be resonant with a vibrational transition of the ground state of molecules, while the visible beam is tuned and used to upconvert the vibrational free induction decay to be resonant with electronic transitions.[12−20] Recently, a femtosecond broadband IR was introduced to mix with a tunable picosecond beam to be doubly resonant with multiple vibrational transitions and electronic transitions simultaneously.[21−28] Although the DR-SFG has provided coupling of electronic and vibrational degrees of freedom, studies of dynamic vibronic coupling at interfaces and surfaces are lacking.

Direct measurements of dynamical vibronic coupling require resonant techniques that interact with both electronic and vibrational transitions, even though two-dimensional electronic spectroscopy could measure vibronic coupling between excitons or different electronic states of systems indirectly in bulk.[29−43] Recent development of 2D electronic-vibrational (2D-EV)[44−46] and 2D vibrational-electronic (2D-VE)[47,48] spectroscopies made it possible that one could directly examine the time-dependent correlation of electronic and vibrational dynamics. These 2D spectroscopies probe the couplings between the electronic and vibrational transition frequencies of molecules in bulk. On the other hand, interface/surface-specific two-dimensional electronic sum frequency generation spectroscopy (2D-ESFG) has emerged as a powerful tool for electronic couplings at interfaces and surfaces.[49,50] However, interface/surface-specific two-dimensional electronic-vibrational sum frequency generation spectroscopy (2D-EVSFG) has not been demonstrated until recently.[51] In this work, we present the develop-

https://doi.org/10.1021/acsphyschemau.3c00011
ACS Phys. Chem Au 2023, 3, 374−385

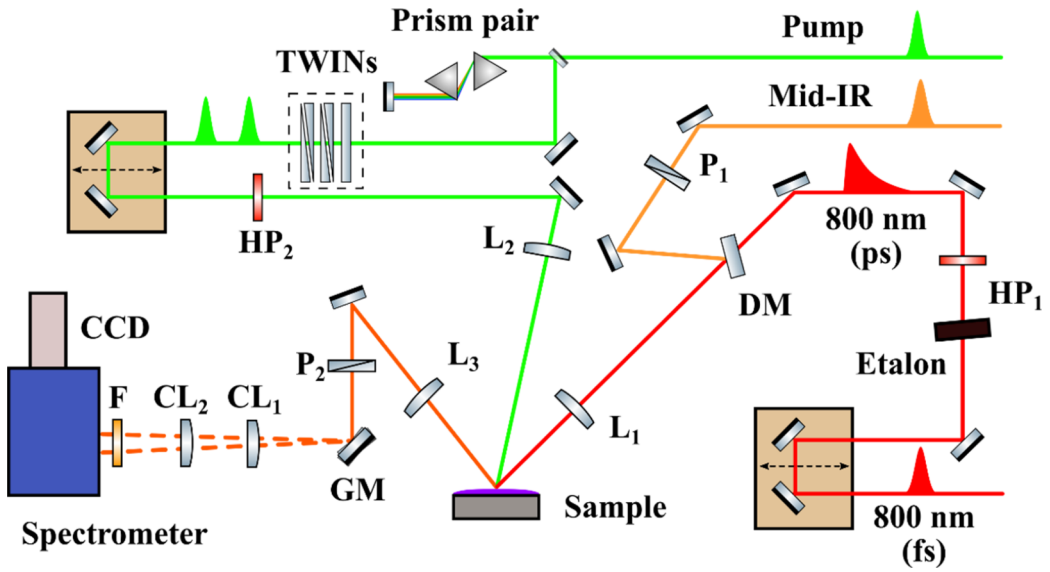

Figure 2. A schematic of 2D-EVSFG experimental setup. CL_1: 25 cm vertically cylindrical lens; CL_2: 10 cm horizontally cylindrical lens; DM: dichroic mirror; F: 780 nm short-pass filter; GM: a galvo mirror; HP_1: half-wave plate for 800 nm; HP_2: half-wave plate for pump; L_1: half-inch 7.5 cm CaF_2 lens; L_2: 1″ 30 cm lens; L_3: 1″ 10 cm lens; P_1: polarizer for mid-IR; P_2: polarizer for signal. The output of a NOPA tunable from 500 to 750 nm was sent to a TWINS system to generate phase-locked double-pump pulses. A mid-IR pulse from an optical parametric amplifier (OPA) and a picosecond 800 nm pulse produced by an etalon were used as a probe. The signal was self-heterodyned and vertically separated onto different CCD strips.

ment of 2D-EVSFG in the time domain for the dynamical interactions of electronic and nucleic motions.

DESIGN PRINCIPLE FOR 2D-EVSFG SPECTROSCOPY

Our 2D-EVSFG experiments consist of four laser beams, including two visible pump beams (k_{V1} and k_{V2}) resonant with electronic transitions, a mid-IR (k_{IR}) resonant with vibrational transitions, and a picosecond 800 nm (k_{ps}) for up-conversion for molecules at interfaces and surfaces. 2D-EVSFG signal is emitted in the k_{sig} direction by satisfying both the energy and momentum conservations ($\mp k_{V1} \pm k_{V2} + k_{IR} + k_{ps}$). The experiments followed a traditional pump−probe geometry for 2D electronic and vibrational spectroscopies.[52−54]

Figure 1(A) (upper) demonstrates the laser pulse sequence for the 2D-EVSFG experiments. The physical time delays of the four laser pulses are defined as the differences between the maxima of the pulse envelopes, specified by a coherent time delay between the pump beams 1 and 2, t_1, a waiting time delay between the pump 2 and the IR, t_w, an up-conversion time delay between the IR and the 800 nm, t_3, and a detection time t between the 800 nm and the signal detection. The response time delays between electric field-matter interactions are specified by t_1', t_2', t_3', and t_4' (Figures 1(A) (bottom)). The first visible pump pulse (k_{V1}) creates a coherent superposition of the ground and excited electronic states. During the coherent time delay, t_1, the second visible pump pulse (k_{V2}) changes the perturbed system into a population state with either the ground or excited state. For a given waiting time delay of t_w, the mid-IR pulse generates vibrational polarization in either the ground or excited state. Within the time delay of t_3, the ps 800 nm beam up-converts the vibrational response of the system, which yields 2D-EVSFG signal at a detection time of t. In our case, the time delay t_3 was set to zero.

In principle, 2D-EVSFG is a fourth-order nonlinear process where the interactions of the four pulses with matter generate a fourth-order nonlinear signal. The signal originates from fourth-order polarization, which is given by the convolution of the fourth-order response function, $R^{(4)}(t_4',t_3',t_2',t_1')$, with the four electric fields as derived in the Supporting Information.[55] Since the electronic responses of molecules interacting with a nonresonant visible light are instantaneous, the fourth-order response function is further expressed as,[56,57]

$$R^{(4)}(t_4', t_3', t_2', t_1') = R^{(3)}(t_3', t_2', t_1')\delta(t_4') \quad (1)$$

Expanding $R^{(3)}(t_3',t_2',t_1')$ yields eight terms grouped into four pairs of complex conjugate field-matter interaction pathways.[58,59] Thus, the 2D-EVSFG enables us to measure the relative strengths with which a vibrational mode is coupled to the solvent on excited states with respect to the ground electronic state at interfaces and surfaces.

Like those in 2D-EV,[60,61] both ground state bleaching (GSB) and excited state absorption (ESA) contribute to responses in 2D-EVSFG. When the pump pair interacts with molecules, the transitions could be a pure electronic transition or a vibronic transition. Figure 1(B) shows energy diagrams for a pure electronic transition (left) and a vibronic transition (right). A pure electronic transition occurs from the ground state |g0> to a higher excited state $|e_1 0'>$ without excitation of any vibrations, while a vibronic transition takes place from ground state |g0> to a higher vibronic state $|e_1 0',\nu>$ accompanied by an excitation of a low frequency ν. It is noted that the vibronic state $|e_1 0',\nu>$ is a Franck−Condon active excited state. When ν is zero, it is a pure electronic transition, namely, $|e_1 0'>$. In other words, any Franck−Condon active low frequency modes could be photo-excited. In the case of GSB contributions, the light-matter interactions further follow a pathway of |g0> → |g1> → |gn>. On the other hand, in the case of ESA contributions, the interactions make a pathway of $|e_1 0'>\rightarrow |e_1 1'> \rightarrow |e_1 n'>$ or $|e_1 0',\nu>\rightarrow |e_1 1',\nu> \rightarrow |e_1 n',\nu>$. |gn> and $|e_1 n',\nu>$ represent virtual states for the ground state and first excited state, respectively.

https://doi.org/10.1021/acsphyschemau.3c00011
ACS Phys. Chem Au 2023, 3, 374−385

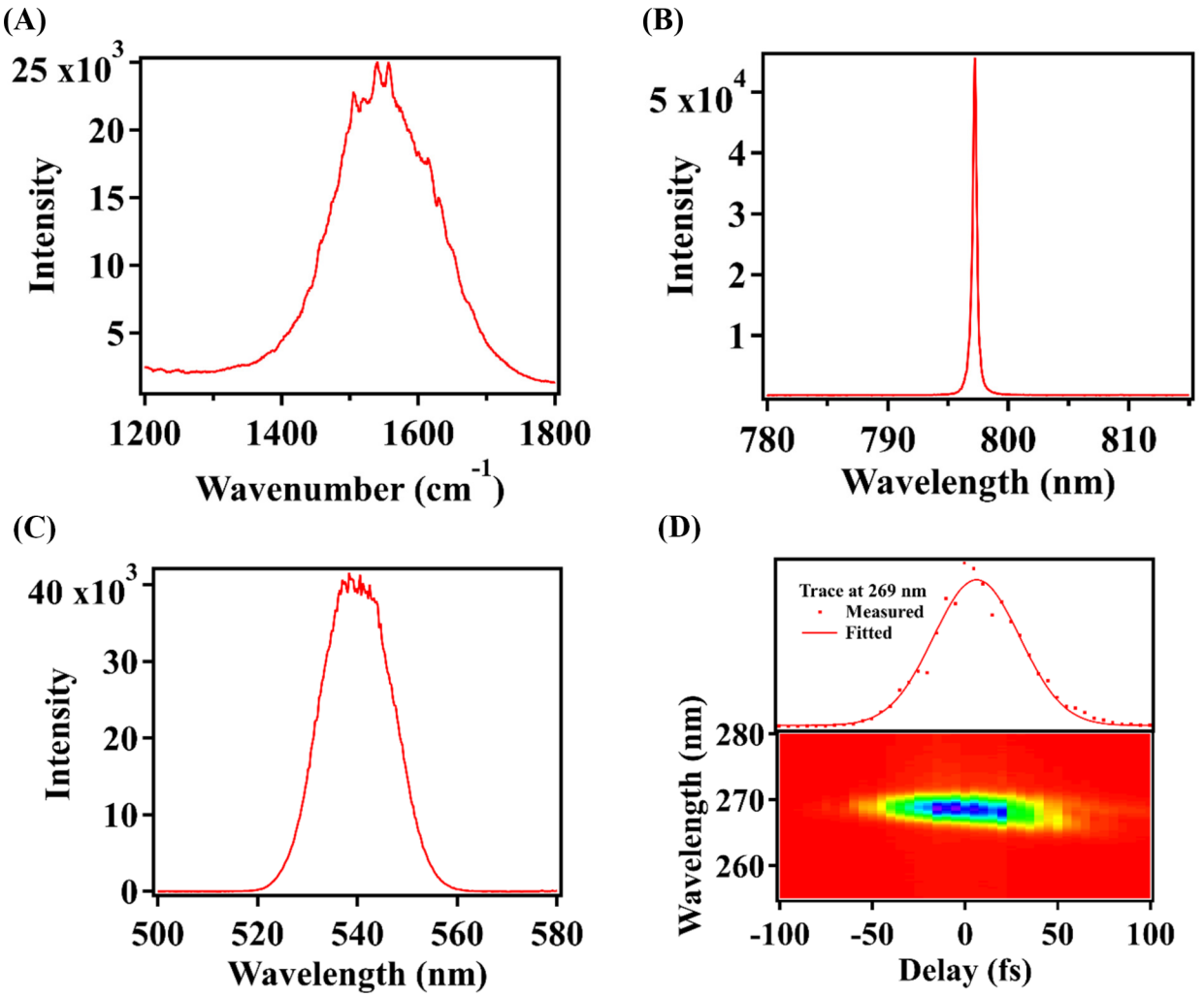

Figure 3. (A) The intensity profiles for the mid-IR beam, (B) the picosecond 800 nm beam, and (C) spectrum of the pump beam, and (D) SHG-FROG result of the pump beam. The pulse duration of the pump beam was ca. 30 fs.

EXPERIMENTAL SECTION

1. Laser Sources for 2D-EVSFG

We adopted a reflection-geometry 2D-EVSFG for studies of liquid interfaces. Figure 2 shows a schematic setup for our 2D-EVSFG experiments. The light source was a 1 kHz Ti:sapphire amplified laser system (UpTek Solutions), which produced ∼100 fs 800 nm pulses with a pulse energy of ∼4 mJ. Three beams, including a femtosecond mid-IR, a picosecond 800 nm, and a femtosecond phase-locked pump pair, were generated from the amplifier as follows:

(a) The femtosecond mid-IR beam. The majority portion of 80% from the amplifier was sent to an optical parametric amplifier (TOPAS-Prime, Light Conversion) (OPA) to generate a broadband mid-IR pulse. The mid-IR of ∼200 cm^{-1} bandwidth was tunable from 2.6 to 20 μm. A typical IR intensity profile was extracted from an SFG spectrum for a p-type GaAs(100) surface by mixing a narrow 800 nm as shown in Figure 3(A). The IR beam at 6.0 μm used in our experiments had an average pulse energy of 6 μJ and a pulse duration of ∼100 fs.

(b) The picosecond 800 nm light. The residual 800 nm light from the TOPAS was used to produce a narrow-band picosecond 800 nm pulse (∼20 μJ) with an air-spaced etalon (SLS Optics). The bandwidth of the picosecond 800 nm pulse was ∼8 cm^{-1}, and its pulse duration was ∼2 ps. A typical spectrum of the picosecond 800 nm pulse is presented in Figure 3(B).

(c) The phase-locked pump pair. The remaining 20% of the output was directed to a home-built noncollinear optical parametric amplifier (NOPA) for a phase-locked pump pair. Figure 3(C) presents a typical spectrum of the pump. The output of the NOPA (tunable from 500−700 nm, 30 nm fwhm, 4 μJ) was compressed with a pair of prisms (LaK21, Newport) to 25−35 fs and characterized by a home-built second-harmonic generation frequency-resolved optical gating (SHG-FROG). The characterization of pump pulses is shown in Figure 3(D). Fitting of a Gaussian function to the SHG trace yields a pulse duration of ca. 30 fs. To generate a phase-locked pump pair, a translating wedge-based identical pulses encoding system (TWINS) was introduced to generate a pair of phase-locked pump pulses with an accuracy of 10 attoseconds. The TWINS was first invented by Cerullo and co-workers.[52,62] The idea of generating two phase-locked collinear pump pulses with very high delay accuracy was based upon the difference in group velocity of ordinary and extraordinary lights in a birefringent crystal. A detailed description of the application of TWINS in 2D spectroscopy can be found in our previous work on the development of 2D-ESFG and 2D-ESHG.[49−51] In our case, a 5 mm X-cut and two pairs of 5 mm Y-cut and 5 mm Z-cut α-BBO crystal wedges were used for the generation of the phase-locked pump pair.[50] The TWINS has the advantages of simplicity, compactness, and low cost.

2. Collection and Detection System

A reflection geometry was used for VSFG and 2D-EVSFG experiments. The picosecond 800 nm and IR beams were combined with a dichroic

https://doi.org/10.1021/acsphyschemau.3c00011
ACS Phys. Chem Au 2023, 3, 374−385

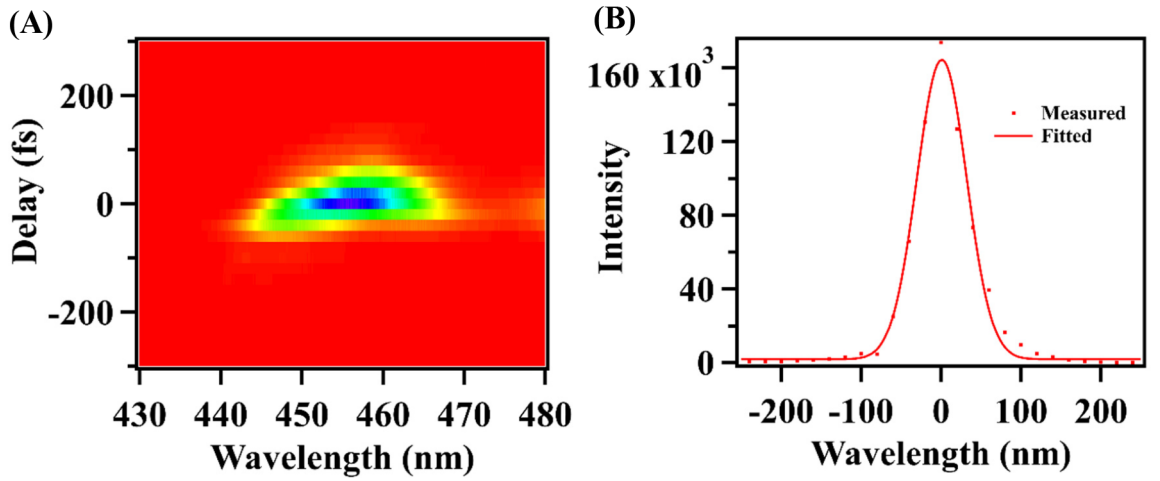

Figure 4. (A) The cross-correlation by third-order signals in GaAs of mid-IR centered at 1550 cm^{-1} and the pump pulse of 540 nm. (B) The determination of the time zero between the mid-IR and pump pulses.

mirror (ISP optics) for a collinear configuration. A CaF_2 lens with a focal length of 75 mm was placed to focus the two beams onto interfaces at an angle of 60° with respect to the surface normal. The incident angle of the pump pulses was set at 50° with respect to the surface normal. The time delay between the 800 nm and the mid-IR was controlled by a translational stage and set to zero for 2D-EVSFG experiments. A programmable motorized translational stage (Klinger) was used to control the time delay, t_w, between the pump pair and the 800 nm/mid-IR pulses. The IR beam path was protected with a sealed box and purged with dry air so that the relative humidity inside was kept less than 1%. Both VSFG and 2D-EVSFG signals were collected in a coherent direction with energy and momentum conservations. 2D-EVSFG signal was emitted in the same phase matching direction as the VSFG since the two phase-locked pump pulses were collinear. The polarization of the two pump beams, 2D-EVSFG/SFG, 800 nm, and IR beams were set to be P-, P-, S-/P-, S-/P-, and P-/P-polarized, respectively. Thus, either PPSSP or PPPPP was used in 2D-EVSFG experiments.

The 2D-EVSFG signals were detected by a spectrometer (Andor-2300i, Princeton Instrument) with a liquid nitrogen-cooled CCD (Princeton Instrument, back-illuminated 1300 × 400). A self-compiled LabVIEW program was compiled to control signal collection and data processing. Each data point was integrated for 10 s. Transient visible pump-VSFG probe experiments were also acquired with the same setup, except the two coherent pump lasers were set to zero.

3. Time Synchronization of the Incident Lights and Signal Acquisition

A pump−probe geometry was adopted for surface-specific 2D-EVSFG spectra. The sampling strategy for 2D-EVSFG was similar to those employed in our previous 2D-ESFG and 2D-ESHG experiments.[49,50] Briefly, a 1 kHz digital signal from the laser system served as a clock for the time synchronization of the acquisition system, followed by a divider to generate a 500 Hz signal for the triggering of the chopper. A lock-in amplifier was synchronized by the chopper with the 500 Hz signal. A single-axis scanning galvanometer system (Thorlabs) was used to spatially separate pump-on and pump-off signals on a charge-coupled device (CCD) chip. The sine-wave output from the lock-in amplifier controlled the movement of the galvo mirror. With fine adjustment of the sine-wave output, the galvo mirror turned up and down with a small angle of around 2° at half of the laser frequency. With a vertically focal cylindrical lens of 25 cm for spatial separation and a horizontally focal cylindrical lens of 10 cm for spectral resolution, pump-on and pump-off signals could be imaged into two spatially separated strips onto the CCD chip.

4. Accurate Determination of the Waiting Time Delay of Zero

In the 2D-EVSFG experiment, the four beams are necessarily overlapped at samples spatially and temporally.

For the spatial overlap, only the pump pair was positioned with either the ps 800 nm or the IR, since the latter two were collinear. This positioning was implemented by ensuring that the beam size of the pump pair was kept much larger than the ps 800 nm.

For the temporal overlap, the time delay (t_3) between the ps 800 nm and the mid-IR was set to zero with a translational stage, where the maximum SFG signal was optimized from a GaAs wafer. Then, the time delay (t_w) between the mid-IR and the pump pulses was determined to ensure accurate control of the physical time delays of the four beams. The coherent time delay, t_1, was incremented in ca. 0.32 fs steps between 0 and 80 fs and is described in the next section. It is important for the dynamical vibronic coupling in 2D-EVSFG to determine the time zero of t_w. To find an accurate time zero of t_w, we measured third-order responses in GaAs with the mid-IR and the visible pump pulse. The third-order responses originated from the interactions of two IR photons and one visible photon with the GaAs, resulting in the wavelength centered at 450 nm as shown in Figure 4(A). Figure 4(B) shows the time trace of the third-order signal at 450 nm. Thus, we are able to find the time zero of t_w.

5. Frequency Calibration of the Coherent Phase-Locked Pulse Pair

In regular 2D electronic spectroscopy experiments, the excitation frequency, ω_e, is generated by Fourier transforming the signal as a function of the coherence time delay, t_1. For the 2D experiments based on programmable pulse shaper systems, such as liquid crystal spatial light modulators (LC-SLMs),[63−65] acousto-optic pulse shapers (AOMs),[43,66−70] and acousto-optic programmable dispersive filters (AOPDFs),[53,71−73] the coherence time, t_1, is perfectly set by the pulse shaper, resulting in accurate excitation frequencies. On the other hand, the coherence time delay was not directly related to the excitation frequency, ω_e, in our case when the pump pair was generated with the TWINS. This lies in the fact that the time delay was varied by following $t_1 = \Delta d(1/v_{ge} - 1/v_{go}) = t_p \tan \alpha(1/v_{ge} - 1/v_{go})$ (v_{ge} and v_{go} are group velocities of ordinary and extraordinary lights) while translating the motor stage of y-cut wedge and changing its thickness by $\Delta d = t_p \tan \alpha$ (t_p is the direct reading of the motor position movement, and α is the apex angle of the wedge).[49−51,62] It is challenging to directly and accurately obtain the wavelength-dependent v_{ge} and v_{go}. As a result, we are not able to extract t_1 directly in time domain for the excitation frequency, ω_e.

Our strategy for extracting the excitation frequency, ω_e, is outlined in Figure 5. To obtain the excitation frequency of the pump pair, we started with t_p for pseudo frequency, ω_p, in the frequency domain.

https://doi.org/10.1021/acsphyschemau.3c00011
ACS Phys. Chem Au 2023, 3, 374−385

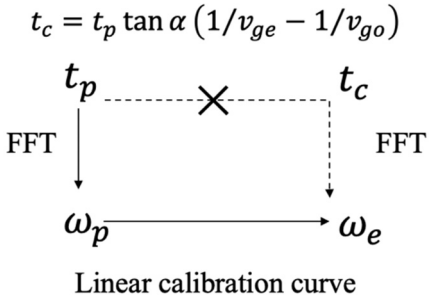

Figure 5. Frequency calibration procedures for a phase-locked pump pair generated by the TWINS.

Experimentally, we measured spectrally resolved interferometry of the two pump pulses by moving the motor position, t_p. The interferometry signal at each frequency is given by

$$I_{SI} = 2\sqrt{I_1}\sqrt{I_2}\cos(\omega t_1 + \Delta\varphi) + I_1^2 + I_2^2$$
$$= 2\sqrt{I_1}\sqrt{I_2}\cos(\omega t_p \tan\alpha(1/v_{ge} - 1/v_{go}) + \Delta\varphi) + \text{D.C.} \quad (2)$$

, where I_1 and I_2 are intensities for the pump pair, v_{ge} and v_{go} are group velocities for extraordinary and ordinary lights, respectively, $\Delta\varphi$ is the phase difference of the pump pair, and D.C. is direct current with frequency-independent intensities for the pump pair. Along the t_p axis, the frequency of cosine fringe at each excitation frequency is $\omega \tan\alpha(1/v_{ge} - 1/v_{go})$, which corresponds to the frequency for t_p, so-called pseudo frequency, ω_p.

To construct a calibration curve for an excitation frequency with a pseudo frequency, three steps are taken as follows:

- Step 1: Take the FFT of the 2D interferogram at each excitation frequency with respect to t_p. A well-defined peak could be obtained at each excitation frequency from Fourier transformation.
- Step 2: Plot the pseudo frequency ω_p as a function of the excitation frequency, ω_e.
- Step 3: Fit to a linear function, $\omega_e = a\omega_p + b$, which is the calibration curve for the real excitation frequency and the pseudo frequency. The intercept, b, is the amount the ω_p axis is shifted with respect to ω_e. Since the pulse pair from the TWINS remains phase-locked, a delay-dependent phase difference results in a partially rotating frame in the 2D-EVSFG experiment.[54,62]

6. Determination of the Absolute Time Zero and Constant Phase of the Phase-Locked Pulse Pair

In a pump−probe 2D-EVSFG geometry, the total phase of the signal, φ_{sig}, is given by,[54]

$$\varphi_{sig} = \pm(\varphi_1 - \varphi_2) + \varphi_S - \varphi_S = \pm(\varphi_1 - \varphi_2) \quad (3)$$

where φ_1, φ_2, and φ_S are the phases of the first pump beam, the second pump beam, and the sum frequency signal, respectively. Thus, the total phase depends on the phase difference in the pump pair, $\Delta\varphi = \varphi_1 - \varphi_2$.

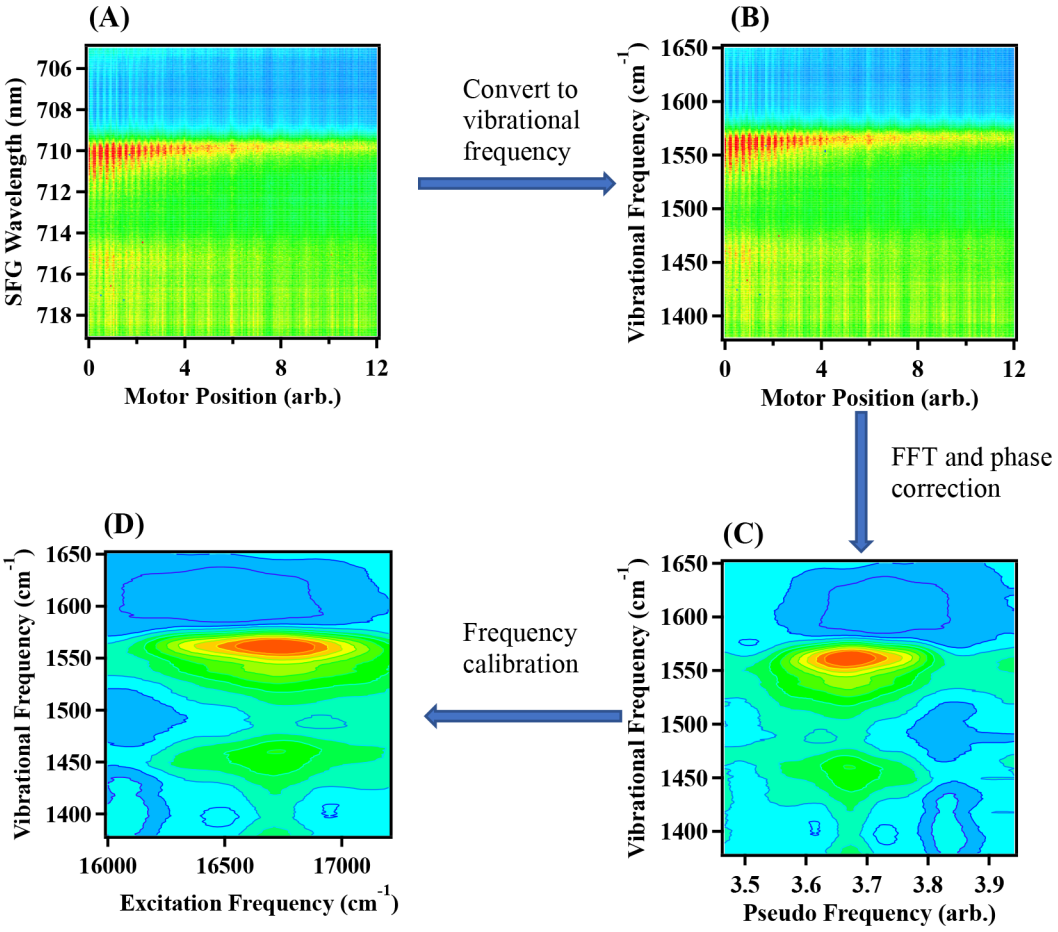

Figure 6. Flowchart of data analysis for 2D-EVSFG of CV at the air/water interface at t_w = 0.5 ps. (A) Pseudo 2D plot of original data of wavelength-dependent 2D-EVSFG signal with motor position. (B) Pseudo 2D plot in vibrational frequency for 2D-EVSFG signal from (A). (C) 2D-EVSFG in terms of pseudo frequency and vibrational frequency. (D) Purely absorptive 2D-EVSFG spectra in terms of excitation frequency and vibrational frequency after $\Delta\varphi_0$ subtraction and calibration procedure of the excitation frequency.

https://doi.org/10.1021/acsphyschemau.3c00011
ACS Phys. Chem Au 2023, 3, 374−385

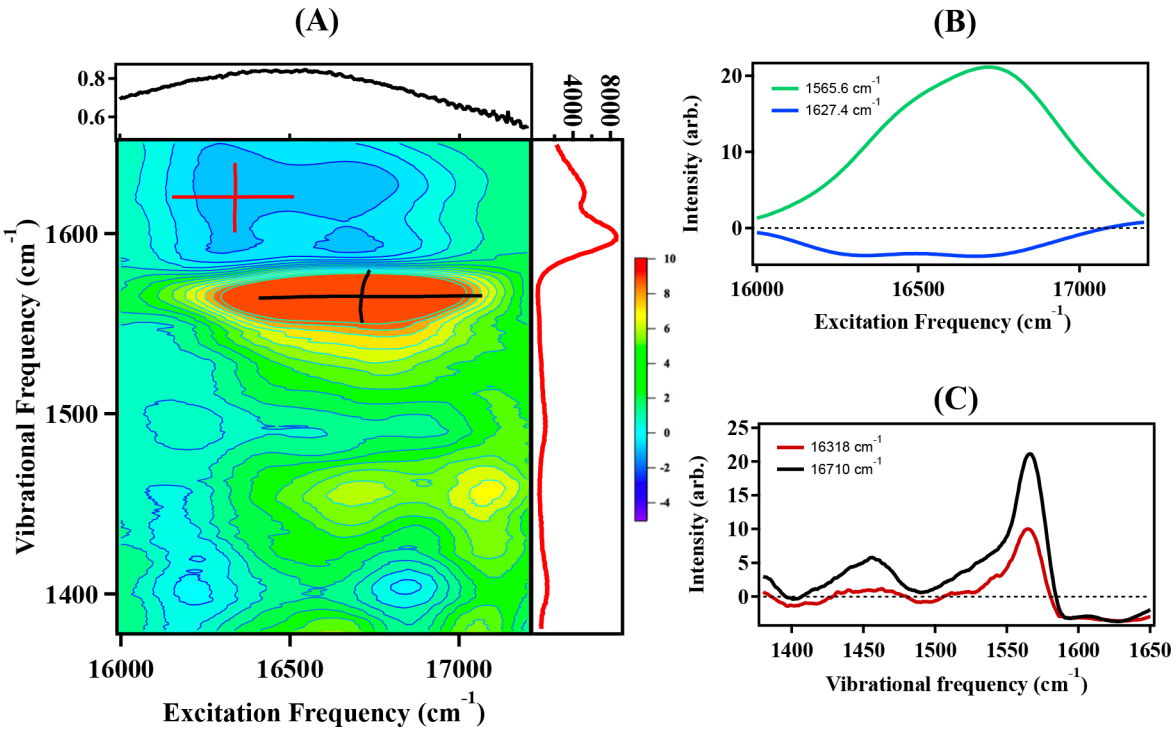

Figure 7. (A) 2D-EVSFG spectra for CV at the air/water interface at a waiting time of 0 fs. The upper inset is the ESHG spectrum of CV under S-in/P-out polarization, and the right inset is the VSFG spectrum of CV under SSP polarization. (B) Sliced spectra along the excitation frequency axis at 1627.4 (GSB) and 1565.6 cm^{-1} (ESA). (C) Sliced spectra along the vibrational frequency axis at 16 318 and 16 710 cm^{-1}.

In pulse shaper systems, a shaper is used to allow arbitrary control over the phases of the pump pair.[54] For the two pump pulses generated by the TWINS, $\Delta\varphi$, the so-called constant phase, is not zero due to their propagations along different crystal axes with higher order dispersion with the same source. To determine the constant phase ($\Delta\varphi_0$) at zero time delay, the delay between the two pulses should be chosen to be as close as possible to zero with very high precision. This is implemented by taking regular linear interferometry of the two pump pulses, as well described by Helbing and Hamm.[74] In making a discrete Fourier transformation, spectral amplitude and phase of linear interferometry are given by

$$A(\omega_p(j)) = |A(\omega_p(j))|\exp(i\Delta\varphi + i\tau_p\omega_p(j)) \quad (4)$$

As seen from eq 4, it is critical to determine the closest zero time delay between the two pump pulses, namely, $\tau_p \approx 0$.

7. Data Analysis

Figure 6(A) shows original 2D-EVSFG data of CV at a waiting of 0.5 ps. To obtain the absorptive 2D-EVSFG spectrum, several steps are taken as follows:

Step 1: Convert the SFG wavelength into its corresponding IR frequency. Thus, we obtain the 2D data as a function of ν_{IR}, as shown in Figure 6(B).

Step 2: Fourier transform the 2D data along t_p and generate the complex absorptive 2D spectrum, as a function of the pseudo excitation frequency, ν_p. The real part of the complex 2D spectrum is purely absorptive, whereas the imaginary part is dispersive.

Step 3: Subtract the relative phase $\Delta\varphi_0$ of the pump pulses by multiplying with the phase term $e^{-i\Delta\varphi_0}$ from eq 4 and obtain the purely absorptive 2D spectrum, as shown in Figure 6(C).

Step 4: Make the calibration procedure of the excitation frequency, ν_e, with the pseudo excitation frequency. Then, one could retrieve in the excitation frequency, as shown in Figure 6(D).

As a result, 2D-EVSFG spectra at each waiting time are plotted as a function of both the excitation and detection frequencies.

Chemicals

Deionized water (18.2 MΩ) was used in all the experiments. Crystal violet (Alfa Aesar) was used as received and dissolved in deionized water with a concentration of 30 μM.

RESULTS AND DISCUSSION

To assist us in identifying peaks in interface-specific two-dimensional EV spectra, we measured one-dimensional interfacial spectra, including interfacial electronic spectra by the broadband electronic second-harmonic generation (ESHG) technique we developed recently[75,76] and interfacial vibrational SFG spectra of CV molecules at the air/water interface. The top inset in Figure 7(A) displays broadband ESHG spectra of CV at the air/water interface under the S-in/P-out polarization combination. Here, "-in" denotes the polarization of an incident light and "-out" is that of an output signal. A broad peak at 16506 cm^{-1} in the S-in/P-out spectrum shows up, which is red-shifted compared to the main peak at 17 152 cm^{-1} in bulk solution.[77] The VSFG spectra were taken from 1380 to 1650 cm^{-1}. The right inset in Figure 7(A) shows VSFG spectra of CV at the air/water interface under the SSP polarization combination. Three main peaks are located at 1623.2, 1597.2, and 1493.8 cm^{-1}, which were attributed to −C=C− stretching, in-the-plane ring stretching and bending, and NR_2 bending and rocking modes, respectively.[78]

Figure 7(A) presents 2D-EVSFG spectra of 30 μM CV molecules at the air/water interface with a waiting time of 0 fs under the polarization combination of PPSSP. Red (positive) and blue (negative) colors denote ESAs and GSBs, respectively. Both negative GSB and positive ESA spectra constitute vibronic transitions (VT) that are related to interfacial electronic absorption of CV. The spectral analysis of the 2D-EVSFG was made as follows:

https://doi.org/10.1021/acsphyschemau.3c00011
ACS Phys. Chem Au 2023, 3, 374−385

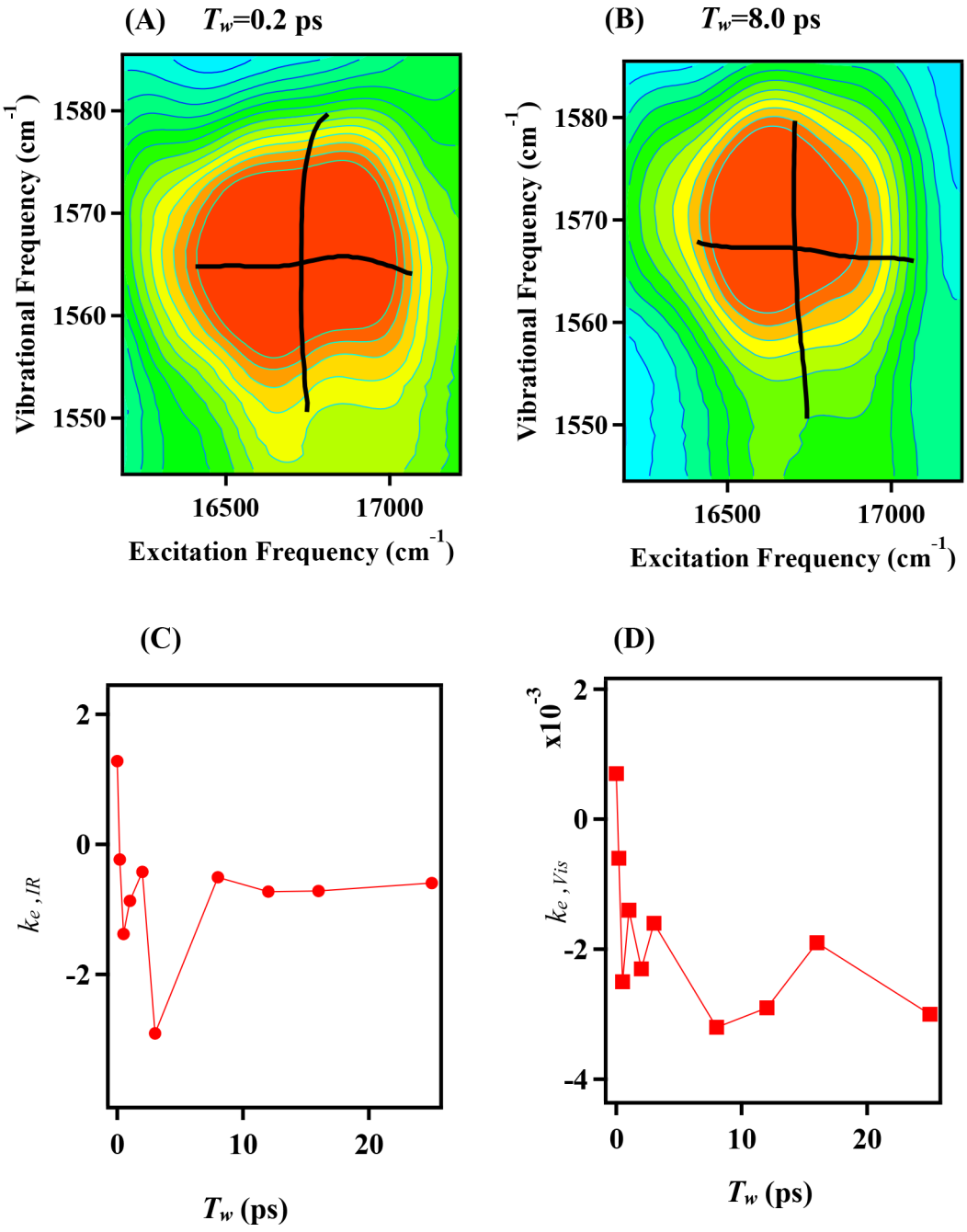

Figure 8. Conditional averages of CLS in 2D-EVSFG spectra at waiting times of 0.2 ps (A) and 8.0 ps (B) for CV molecules at the air/water interface under PPSSP. $k_{e,IR}$ (C) and $k_{e,Vis}$ (D) as a function of a waiting time, T_w.

(1) Along the excitation frequency axis, two main VT peaks occur at 16 318 and 16 710 cm^{-1} at the vibrational frequency of 1627.4 cm^{-1} in the GSB, as shown in Figure 7(B). Compared with the broad peak at 16 506 cm^{-1} in the one-dimensional electronic spectrum, the 2D-EVSFG presents more prominent VT peaks. If the lowest energy level of 16 318 cm^{-1} was considered to be the transition from |g0> to |e0′>, a vibrational frequency of 392 cm^{-1} was excited for the transition of 16 710 cm^{-1}. We further found that the intensity ratio at 16 710 and 16 318 cm^{-1} was 1.02:1.00. Such a large transition at this vibrational mode suggests non-Condon participation in the vibronic transition since a large reorganization of Franck−Condon excitation for CV could not possibly happen. On the other hand, at the vibrational frequency of 1565.6 cm^{-1} in the ESA, two slightly shifted VT peaks appear at 16 372 and 16 717 cm^{-1} but exhibit much stronger intensities than their counterparts in the GSB. It is noted that the vibronic absorption peaks for CV molecules at the interface in 2D-EVSFG are more prominent, even though the vibrational peaks are similar.[79] These features suggest that 2D-EVSFG provides unique local properties at interfaces.

(2) Along the vibrational frequency axis for the excitation frequencies of 16 318 and 16 710 cm^{-1} as shown in Figure 7(C), the two negative peaks at 1628.3 and 1591.3 cm^{-1} were attributed to GSB, which is consistent with those from one-dimensional VSFG in the right inset in Figure 7(A). Since VSFG is both Raman- and IR-active, the GSB

https://doi.org/10.1021/acsphyschemau.3c00011
ACS Phys. Chem Au 2023, 3, 374−385

shows two peaks at 1628.3 and 1591.3 cm^{-1} in 2D-EVSFG, instead of one peak at 1595 cm^{-1} in 2D-EV.[79] On the other hand, three positive peaks occur at 1565.6, 1528.3, and 1454.8 cm^{-1}. The first and third peaks were due to the vibrational transitions of 1597.2 and 1493.8 cm^{-1} in the excited state of CV.[79] The ESA peak for 1628.3 cm^{-1} overlapped with the GSB peak of 1591.3 cm^{-1} and could not be differentiated in our case. The spectral red shift between the GSB and ESA vibrational peaks was found to be close to 31.6 and 39.0 cm^{-1}. The 2D-EVSFG data offer vibrational information on both excited states and ground state as compared with the traditional doubly resonant sum frequency generation.

Interactions between a chromophore and its surrounding solvent lead to spectral diffusion processes in electronic transitions, vibrational transitions, or both. For electronic-vibrational transitions, solvent interactions are related to the couplings of the electronic and vibrational degrees of freedom with solvent modes. Previous theories state that the fluctuations in the electronic and vibrational motions are intimately correlated through the energy fluctuations of the vibrations on the electronic excited state at an early waiting time, before other relaxation processes take place.[45] The center line slopes (CLSs) were often used to quantify the energy fluctuations. From CLS values in 2D-EVSFG peaks, one might be able to directly measure the relative strengths with which a vibrational mode is coupled to the solvent on excited states with respect to the ground electronic state at interfaces and surfaces. Following the pioneering work for 2D-EV from the Fleming group,[45,79] we defined the following four conditional averages of CLSs in 2D-EVSFG: $k_{g,Vis}$ and $k_{g,IR}$ for GSB peaks and $k_{e,Vis}$ and $k_{e,IR}$ for ESA peaks. The $k_{g,IR}$ and $k_{e,IR}$ are the conditional averages of CLSs with respect to the vibrational frequency, while the $k_{g,Vis}$ and $k_{e,Vis}$ are the conditional averages of CLSs with respect to the excitation frequency. The magnitude of the CLSs could be utilized to compare the relative strengths for a vibration that is coupled with its surrounding solvent on an excited state with respect to the ground state.

Figure 7(A) shows solvent correlations from 2D-EVSFG spectra at a waiting time of 0 fs for CV molecules at the air/water interface under PPSSP. The values for $k_{g,Vis}$ and $k_{g,IR}$, at the GSB peak of (16 318 cm^{-1}, 1627.4 cm^{-1}), were estimated to be 5.39 $\times 10^{-4}$ and 0.216, respectively, while those for $k_{e,Vis}$, and $k_{e,IR}$ at the ESA peak of (16 709 cm^{-1}, 1565.6 cm^{-1}) were 7.52 $\times 10^{-4}$ and 1.305, respectively. All the CLS values exhibit positive solvent correlations at the air/water interface. Based on the analysis in 2D-EV,[45] we attempted to estimate the vibrational solvent coupling for the zeroth and first vibrational levels on the electronic state with respect to those on the ground state, being on the order of 0.216 and 0.382. The former one is much smaller than that of 1.5 in bulk methanol.[79] Such a low value at the interface suggests that the solvent reorganization energy of the zeroth vibrational level of the excited state is less than that on the ground state. These preliminary results show that 2D-EVSFG could be used to describe the strength of the vibrational coupling to the bath on the electronic excited state for a given vibrational mode at interfaces.

The advantage of 2D-EVSFG is that the time evolution of photoinduced electronic states is tracked from time-dependent spectra, as compared with steady-state double-resonance SFG. With different waiting times, we are able to monitor the structural evolution of molecules at interfaces. Figure 8 shows 2D-EVSFG spectra at the ESA peak of (16 709 cm^{-1}, 1565.6 cm^{-1}) for 30 μM CV at the air/water interface at two different waiting times of 0.20 (A) and 8.00 ps (B) under PPSSP. The CLSs for these waiting times were also appended in Figure 8(A,B). Furthermore, the $k_{e,Vis}$, and $k_{e,IR}$ values were extracted for different waiting times as shown in Figures 8(C,D). Even though the data for the CLSs were not satisfactory, qualitative comparisons showed that these kinetic behaviors of CV at the air/water interface are significantly different from those in bulk methanol.[45] Thus, time-dependent 2D-EVSFG could help us depict dynamical vibronic coupling of molecules at interfaces.

SUMMARY AND PERSPECTIVES

In summary, we have successfully developed an interface/surface-specific 2D-EVSFG spectroscopy. The 2D-EVSFG spectrometer was based upon four laser beams, including a phase-locked pump pair, a mid-IR, and a picosecond narrow beam. A translating wedge-based identical pulses encoding system (TWINS) was used for a phase-locked pulse pair for coherent excitation. The frequency calibration of the pump pair and its zero time delay determination as well as constant phase were implemented from spectrally resolved interferometry measurements. The synchronization of the four lasers and signal detection of 2D-EVSFG were achieved. Data analysis has been described step by step. Furthermore, we have applied 2D-EVSFG into crystal violet (CV) molecules at the air/water interface.

From the 2D-EVSFG spectra, we have demonstrated vibronic coupling and solvent correlation of CV at the air/water interface. The two vibronic absorption peaks for CV molecules at the interface from the 2D-EVSFG experiments were found to be more prominent than their counterparts in bulk from 2D-EV. The 2D-EVSFG also offers vibrational information on both excited states and the ground state as compared with the traditional doubly resonant sum frequency generation. Quantitative analysis of the vibronic peaks in 2D-EVSFG suggested that a non-Condon process participates in the photoexcitation of CV at the interface. We further revealed vibrational solvent coupling for the zeroth level on the electronic state with respect to those on the ground state, being on the order of 0.216 and related to a change in its solvent reorganization energy. The change in the solvent reorganization energy at the interface is much smaller than that in bulk methanol. Time-dependent 2D-EVSFG CLSs showed that kinetic behaviors of CV at the air/water interface are significantly different from those in bulk methanol.

With this emerging technique, our next aim is to utilize different polarization combinations to obtain relative orientations of vibrational dipoles and electronic dipoles. 2D-EVSFG measures electronic-vibrational responses under electronic excitations at interfaces. In other words, 2D-EVSFG signal for a particular vibrational dipole could be enhanced or suppressed by experimentally setting the polarization combination of the incident and the detected electric fields. Currently, the main challenge in the 2D-EVSFG with the TWINS method is that it is time-consuming. The frequency calibration of a pump pair and the determination of its time zero are tedious. In addition, the TWINS requires a high-quality spatial mode of a pump source. Phase cycling is a promising alternative, which is often used in ultrafast 2D experiments. Our next plan is to introduce the phase cycling method into 2D-EVSFG experiments. In addition, the pump−probe configuration significantly simplified the experimental implementations of the 2D-EVSFG but left one disadvantage with unwanted transient absorption backgrounds.

https://doi.org/10.1021/acsphyschemau.3c00011
ACS Phys. Chem Au 2023, 3, 374−385

Our ultrafast 2D-EVSFG experiments not only offer vibrational information on both excited states and ground state as compared with the traditional doubly resonant sum frequency generation and electronic-vibrational coupling but also provide vibronic coupling, a dynamical solvent effect, and time evolution of vibronic coupling at interfaces. This time-resolved and interface-specific electronic-vibrational spectroscopy is readily applied to reveal the structure and dynamics of interface and surface species in the fields of environment, materials, catalysis, and biology.

■ ASSOCIATED CONTENT

Supporting Information

The Supporting Information is available free of charge at https://pubs.acs.org/doi/10.1021/acsphyschemau.3c00011.

Derivation of fourth-order response function (PDF)

■ AUTHOR INFORMATION

Corresponding Author

Yi Rao − *Department of Chemistry and Biochemistry, Utah State University, Logan, Utah 84322, United States;* orcid.org/0000-0001-9882-1314; Email: yi.rao@usu.edu

Authors

Zhi-Chao Huang-Fu − *Department of Chemistry and Biochemistry, Utah State University, Logan, Utah 84322, United States*

Yuqin Qian − *Department of Chemistry and Biochemistry, Utah State University, Logan, Utah 84322, United States*

Gang-Hua Deng − *Department of Chemistry and Biochemistry, Utah State University, Logan, Utah 84322, United States*

Tong Zhang − *Department of Chemistry and Biochemistry, Utah State University, Logan, Utah 84322, United States*

Sydney Schmidt − *Department of Chemistry and Biochemistry, Utah State University, Logan, Utah 84322, United States*

Jesse Brown − *Department of Chemistry and Biochemistry, Utah State University, Logan, Utah 84322, United States*

Complete contact information is available at: https://pubs.acs.org/10.1021/acsphyschemau.3c00011

Author Contributions

Z.-C.H.-F. and Y.Q. contributed equally to this work. CRediT: **Zhi-Chao Huang-Fu** data curation (equal), investigation (equal), methodology (equal), writing-original draft (equal); **Yuqin Qian** data curation (equal), formal analysis (equal), investigation (equal), visualization (equal), writing-original draft (equal); **Gang-Hua Deng** data curation (equal), investigation (equal), methodology (equal); **Tong Zhang** data curation (equal), formal analysis (equal), investigation (equal), validation (equal), visualization (equal), writing-original draft (equal); **Sydney Schmidt** formal analysis (equal), investigation (equal), writing-original draft (equal); **Jesse B. Brown** investigation (equal), writing-original draft (equal); **Yi Rao** conceptualization (equal), investigation (equal), project administration (equal), supervision (equal), writing-review & editing (equal).

Notes

The authors declare no competing financial interest.

■ ACKNOWLEDGMENTS

This material is based upon work supported by the National Science Foundation under Grant No. [2045084].

■ REFERENCES

(1) Adamson, A. W.; Gast, A. P. *Physical chemistry of surfaces*, 6th ed.; Wiley-Interscience: New York, 1997; Vol. *150*.

(2) Butt, H.-J.; Graf, K.; Kappl, M. *Physics and chemistry of interfaces*, 3rd ed.; John Wiley & Sons, 2013.

(3) Chen, X.; Wang, K.; Beard, M. C. Ultrafast probes at the interfaces of solar energy conversion materials. *Phys. Chem. Chem. Phys.* **2019**, *21* (30), 16399−16407.

(4) Manzano-Agugliaro, F.; Fernández-García, A. *Surfaces and Interfaces for Renewable Energy*; MDPI AG, 2020.

(5) Grassian, V. H. Physical Chemistry of Environmental Interfaces and the Environment in Physical Chemistry-A Career Perspective. *J. Phys. Chem. C* **2022**, *126* (30), 12320−12326.

(6) Subir, M.; Rao, Y. *Environmental Interfacial Spectroscopy*; American Chemical Society: Washington DC, 2022.

(7) Chen, S.; Qi, Y.; Li, C.; Domen, K.; Zhang, F. Surface Strategies for Particulate Photocatalysts toward Artificial Photosynthesis. *Joule* **2018**, *2* (11), 2260−2288.

(8) Warburton, R. E.; Hutchison, P.; Jackson, M. N.; Pegis, M. L.; Surendranath, Y.; Hammes-Schiffer, S. Interfacial Field-Driven Proton-Coupled Electron Transfer at Graphite-Conjugated Organic Acids. *J. Am. Chem. Soc.* **2020**, *142* (49), 20855−20864.

(9) Ge, A.; Kastlunger, G.; Meng, J.; Lindgren, P.; Song, J.; Liu, Q.; Zaslavsky, A.; Lian, T.; Peterson, A. A. On the Coupling of Electron Transfer to Proton Transfer at Electrified Interfaces. *J. Am. Chem. Soc.* **2020**, *142* (27), 11829−11834.

(10) Li, B.; Zhao, J.; Onda, K.; Jordan, K. D.; Yang, J.; Petek, H. Ultrafast Interfacial Proton-Coupled Electron Transfer. *Science* **2006**, *311* (5766), 1436−1440.

(11) Shen, Y. R. Surface-Properties Probed by 2nd-Harmonic and Sum-Frequency Generation. *Nature* **1989**, *337* (6207), 519−525.

(12) Huang, J. Y.; Shen, Y. R. Theory of doubly resonant infrared-visible sum-frequency and difference-frequency generation from adsorbed molecules. *Phys. Rev. A* **1994**, *49* (5), 3973−3981.

(13) Raschke, M. B.; Hayashi, M.; Lin, S. H.; Shen, Y. R. Doubly-resonant sum-frequency generation spectroscopy for surface studies. *Chem. Phys. Lett.* **2002**, *359* (5), 367−372.

(14) Hayashi, M.; Lin, S. H.; Raschke, M. B.; Shen, Y. R. A Molecular Theory for Doubly Resonant IR-UV-vis Sum-Frequency Generation. *J. Phys. Chem. A* **2002**, *106* (10), 2271−2282.

(15) Wu, D.; Deng, G.-H.; Guo, Y.; Wang, H.-f. Observation of the Interference between the Intramolecular IR-Visible and Visible-IR Processes in the Doubly Resonant Sum Frequency Generation Vibrational Spectroscopy of Rhodamine 6G Adsorbed at the Air/Water Interface. *J. Phys. Chem. A* **2009**, *113* (21), 6058−6063.

(16) Rao, Y.; Turro, N. J.; Eisenthal, K. B. Solvation Dynamics at the Air/Water Interface with Time-Resolved Sum-Frequency Generation. *J. Phys. Chem. C* **2010**, *114* (41), 17703−17708.

(17) Bozzini, B.; D'Urzo, L.; Mele, C.; Busson, B.; Humbert, C.; Tadjeddine, A. Doubly Resonant Sum Frequency Generation Spectroscopy of Adsorbates at an Electrochemical Interface. *J. Phys. Chem. C* **2008**, *112* (31), 11791−11795.

(18) Belkin, M. A.; Shen, Y. R. Doubly Resonant IR-UV Sum-Frequency Vibrational Spectroscopy on Molecular Chirality. *Phys. Rev. Lett.* **2003**, *91* (21), 213907.

(19) Han, S. H.; Ji, N.; Belkin, M. A.; Shen, Y. R. Sum-frequency spectroscopy of electronic resonances on a chiral surface monolayer of bi-naphthol. *Phys. Rev. B* **2002**, *66* (16), 165415.

(20) Chou, K. C.; Westerberg, S.; Shen, Y. R.; Ross, P. N.; Somorjai, G. A. Probing the charge-transfer state of CO on Pt(111) by two-dimensional infrared-visible sum frequency generation spectroscopy. *Phys. Rev. B* **2004**, *69* (15), 153413.

(21) Sengupta, S.; Bromley, L., III; Velarde, L. Aggregated States of Chalcogenorhodamine Dyes on Nanocrystalline Titania Revealed by

Doubly Resonant Sum Frequency Spectroscopy. *J. Phys. Chem. C* **2017**, *121* (6), 3424−3436.
(22) Busson, B.; Farhat, M.; Nini Teunda, P.-J.; Roy, S.; Jarisz, T.; Hore, D. K. All-experimental analysis of doubly resonant sum-frequency generation spectra: Application to aggregated rhodamine films. *J. Chem. Phys.* **2021**, *154* (22), 224704.
(23) Elsenbeck, D.; Das, S. K.; Velarde, L. Substrate influence on the interlayer electron-phonon couplings in fullerene films probed with doubly-resonant SFG spectroscopy. *Phys. Chem. Chem. Phys.* **2017**, *19* (28), 18519−18528.
(24) Wang, J.; Wu, X.; He, Y.; Guo, W.; Zhang, Q.; Wang, Y.; Wang, Z. Investigation of the Electronic Structure of CdS Nanoparticles with Sum Frequency Generation and Photoluminescence Spectroscopy. *J. Phys. Chem. C* **2019**, *123* (45), 27712−27716.
(25) Busson, B. Doubly resonant SFG and DFG spectroscopies: An analytic model for data analysis including distorted and rotated vibronic levels. I. Theory. *J. Chem. Phys.* **2020**, *153* (17), 174701.
(26) Busson, B. Doubly resonant SFG and DFG spectroscopies: An analytic model for data analysis including distorted and rotated vibronic levels. II. Applications. *J. Chem. Phys.* **2020**, *153* (17), 174702.
(27) Busson, B. All-experimental analysis of doubly resonant sum-frequency generation spectra for Franck-Condon and Herzberg-Teller vibronic modes. *J. Chem. Phys.* **2022**, *156* (20), 204704.
(28) Yang, S.; Noguchi, H.; Uosaki, K. Electronic Structure of the CO/Pt(111) Electrode Interface Probed by Potential-Dependent IR/Visible Double Resonance Sum Frequency Generation Spectroscopy. *J. Phys. Chem. C* **2015**, *119* (46), 26056−26063.
(29) Ginsberg, N. S.; Cheng, Y.-C.; Fleming, G. R. Two-Dimensional Electronic Spectroscopy of Molecular Aggregates. *Acc. Chem. Res.* **2009**, *42* (9), 1352−1363.
(30) Moody, G.; Cundiff, S. T. Advances in multi-dimensional coherent spectroscopy of semiconductor nanostructures. *Advances in Physics: X* **2017**, *2* (3), 641−674.
(31) Dean, J. C.; Scholes, G. D. Coherence Spectroscopy in the Condensed Phase: Insights into Molecular Structure, Environment, and Interactions. *Acc. Chem. Res.* **2017**, *50* (11), 2746−2755.
(32) Fuller, F. D.; Ogilvie, J. P. Experimental Implementations of Two-Dimensional Fourier Transform Electronic Spectroscopy. *Annu. Rev. Phys. Chem.* **2015**, *66* (1), 667−690.
(33) Cho, M.; Brixner, T.; Stiopkin, I.; Vaswani, H.; Fleming, G. R. Two Dimensional Electronic Spectroscopy of Molecular Complexes. *Journal of the Chinese Chemical Society* **2006**, *53* (1), 15−24.
(34) Schlau-Cohen, G. S.; Ishizaki, A.; Fleming, G. R. Two-dimensional electronic spectroscopy and photosynthesis: Fundamentals and applications to photosynthetic light-harvesting. *Chem. Phys.* **2011**, *386* (1), 1−22.
(35) Milota, F.; Sperling, J.; Nemeth, A.; Mančal, T.; Kauffmann, H. F. Two-Dimensional Electronic Spectroscopy of Molecular Excitons. *Acc. Chem. Res.* **2009**, *42* (9), 1364−1374.
(36) Harel, E.; Engel, G. S. Quantum Coherence Spectroscopy Reveals Complex Dynamics in Bacterial Light-Harvesting Complex 2 (LH2). *Proc. Natl. Acad. Sci. U. S. A.* **2012**, *109* (3), 706−711.
(37) Jonas, D. M. Vibrational and Nonadiabatic Coherence in 2D Electronic Spectroscopy, the Jahn-Teller Effect, and Energy Transfer. *Annu. Rev. Phys. Chem.* **2018**, *69* (1), 327−352.
(38) Halpin, A.; Johnson, P. J.; Tempelaar, R.; Murphy, R. S.; Knoester, J.; Jansen, T. L.; Miller, R. D. Two-Dimensional Spectroscopy of a Molecular Dimer Unveils the Effects of Vibronic Coupling on Exciton Coherences. *Nature Chem.* **2014**, *6* (3), 196.
(39) Schröter, M.; Alcocer, M. J. P.; Cogdell, R. J.; Kühn, O.; Zigmantas, D. Origin of the Two Bands in the B800 Ring and Their Involvement in the Energy Transfer Network of Allochromatium vinosum. *J. Phys. Chem. Lett.* **2018**, *9* (6), 1340−1345.
(40) Zhao, W.; Qin, Z.; Zhang, C.; Wang, G.; Huang, X.; Li, B.; Dai, X.; Xiao, M. Optical Gain from Biexcitons in CsPbBr3 Nanocrystals Revealed by Two-dimensional Electronic Spectroscopy. *J. Phys. Chem. Lett.* **2019**, *10* (6), 1251−1258.
(41) Wells, K. L.; Lambrev, P. H.; Zhang, Z.; Garab, G.; Tan, H.-S. Pathways of energy transfer in LHCII revealed by room-temperature 2D electronic spectroscopy. *Phys. Chem. Chem. Phys.* **2014**, *16* (23), 11640−11646.
(42) Borrego-Varillas, R.; Nenov, A.; Ganzer, L.; Oriana, A.; Manzoni, C.; Tolomelli, A.; Rivalta, I.; Mukamel, S.; Garavelli, M.; Cerullo, G. Two-Dimensional UV Spectroscopy: a New Insight into the Structure and Dynamics of Biomolecules. *Chemical Science* **2019**, *10* (43), 9907−9921.
(43) Tian, P.; Keusters, D.; Suzaki, Y.; Warren, W. S. Femtosecond Phase-Coherent Two-Dimensional Spectroscopy. *Science* **2003**, *300* (5625), 1553−1555.
(44) Oliver, T. A. A.; Lewis, N. H. C.; Fleming, G. R. Correlating the motion of electrons and nuclei with two-dimensional electronic-vibrational spectroscopy. *Proc. Natl. Acad. Sci. U. S. A.* **2014**, *111* (28), 10061−10066.
(45) Lewis, N. H. C.; Dong, H.; Oliver, T. A. A.; Fleming, G. R. Measuring correlated electronic and vibrational spectral dynamics using line shapes in two-dimensional electronic-vibrational spectroscopy. *J. Chem. Phys.* **2015**, *142* (17), 174202.
(46) Gaynor, J. D.; Courtney, T. L.; Balasubramanian, M.; Khalil, M. Fourier transform two-dimensional electronic-vibrational spectroscopy using an octave-spanning mid-IR probe. *Optics letters* **2016**, *41* (12), 2895−2898.
(47) Courtney, T. L.; Fox, Z. W.; Slenkamp, K. M.; Khalil, M. Two-dimensional vibrational-electronic spectroscopy. *J. Chem. Phys.* **2015**, *143* (15), 154201.
(48) Courtney, T. L.; Fox, Z. W.; Estergreen, L.; Khalil, M. Measuring coherently coupled intramolecular vibrational and charge-transfer dynamics with two-dimensional vibrational-electronic spectroscopy. *journal of physical chemistry letters* **2015**, *6* (7), 1286−1292.
(49) Deng, G.-H.; Qian, Y.; Wei, Q.; Zhang, T.; Rao, Y. Interface-Specific Two-Dimensional Electronic Sum Frequency Generation Spectroscopy. *J. Phys. Chem. Lett.* **2020**, *11* (5), 1738−1745.
(50) Deng, G.-H.; Wei, Q.; Qian, Y.; Zhang, T.; Leng, X.; Rao, Y. Development of interface-/surface-specific two-dimensional electronic spectroscopy. *Rev. Sci. Instrum.* **2021**, *92* (2), 023104.
(51) Deng, G.-H.; Qian, Y.; Zhang, T.; Han, J.; Chen, H.; Rao, Y. Two-dimensional electronic-vibrational sum frequency spectroscopy for interactions of electronic and nuclear motions at interfaces. *Proc. Natl. Acad. Sci. U. S. A.* **2021**, *118* (34), No. e2100608118.
(52) Réhault, J.; Maiuri, M.; Oriana, A.; Cerullo, G. Two-Dimensional Electronic Spectroscopy with Birefringent Wedges. *Rev. Sci. Instrum.* **2014**, *85* (12), 123107.
(53) Myers, J. A.; Lewis, K. L. M.; Tekavec, P. F.; Ogilvie, J. P. Two-color two-dimensional Fourier transform electronic spectroscopy with a pulse-shaper. *Opt. Express* **2008**, *16* (22), 17420−17428.
(54) Shim, S.-H.; Zanni, M. T. How to Turn Your Pump-Probe Instrument into a Multidimensional Spectrometer: 2D IR and Vis Spectroscopiesvia Pulse Shaping. *Phys. Chem. Chem. Phys.* **2009**, *11* (5), 748−761.
(55) Cho, M. *Two-dimensional optical spectroscopy*; CRC press, 2009.
(56) Xiong, W.; Laaser, J. E.; Mehlenbacher, R. D.; Zanni, M. T. Adding a dimension to the infrared spectra of interfaces using heterodyne detected 2D sum-frequency generation (HD 2D SFG) spectroscopy. *Proc. Natl. Acad. Sci. U. S. A.* **2011**, *108* (52), 20902−20907.
(57) Laaser, J. E.; Xiong, W.; Zanni, M. T. Time-Domain SFG Spectroscopy Using Mid-IR Pulse Shaping: Practical and Intrinsic Advantages. *J. Phys. Chem. B* **2011**, *115* (11), 2536−2546.
(58) Mukamel, S. *Principles of Nonlinear Optical Spectroscopy*; Oxford University Press, 1995.
(59) Hamm, P.; Zanni, M. *Concepts and Methods of 2D Infrared Spectroscopy*; Cambridge University Press, 2011.
(60) Oliver, T. A. A.; Lewis, N. H. C.; Fleming, G. R. Correlating the motion of electrons and nuclei with two-dimensional electronic−vibrational spectroscopy. *Proc. Natl. Acad. Sci. U. S. A.* **2014**, *111* (28), 10061−10066.
(61) Gaynor, J. D.; Khalil, M. Signatures of vibronic coupling in two-dimensional electronic-vibrational and vibrational-electronic spectroscopies. *J. Chem. Phys.* **2017**, *147* (9), 094202.

(62) Brida, D.; Manzoni, C.; Cerullo, G. Phase-locked pulses for two-dimensional spectroscopy by a birefringent delay line. *Opt. Lett.* **2012**, *37* (15), 3027−3029.
(63) Grumstrup, E. M.; Shim, S.-H.; Montgomery, M. A.; Damrauer, N. H.; Zanni, M. T. Facile collection of two-dimensional electronic spectra using femtosecond pulse-shaping technology. *Opt. Express* **2007**, *15* (25), 16681−16689.
(64) Vaughan, J. C.; Hornung, T.; Stone, K. W.; Nelson, K. A. Coherently Controlled Ultrafast Four-Wave Mixing Spectroscopy. *J. Phys. Chem. A* **2007**, *111* (23), 4873−4883.
(65) Gundogdu, K.; Stone, K. W.; Turner, D. B.; Nelson, K. A. Multidimensional coherent spectroscopy made easy. *Chem. Phys.* **2007**, *341* (1), 89−94.
(66) Rock, W.; Li, Y.-L.; Pagano, P.; Cheatum, C. M. 2D IR Spectroscopy using Four-Wave Mixing, Pulse Shaping, and IR Upconversion: A Quantitative Comparison. *J. Phys. Chem. A* **2013**, *117* (29), 6073−6083.
(67) Kearns, N. M.; Mehlenbacher, R. D.; Jones, A. C.; Zanni, M. T. Broadband 2D electronic spectrometer using white light and pulse shaping: noise and signal evaluation at 1 and 100 kHz. *Opt. Express* **2017**, *25* (7), 7869−7883.
(68) Karthick Kumar, S. K.; Tamimi, A.; Fayer, M. D. Comparisons of 2D IR measured spectral diffusion in rotating frames using pulse shaping and in the stationary frame using the standard method. *J. Chem. Phys.* **2012**, *137* (18), 184201.
(69) Shim, S.-H.; Strasfeld, D. B.; Ling, Y. L.; Zanni, M. T. Automated 2D IR spectroscopy using a mid-IR pulse shaper and application of this technology to the human islet amyloid polypeptide. *Proc. Natl. Acad. Sci. U. S. A.* **2007**, *104* (36), 14197−14202.
(70) Middleton, C. T.; Woys, A. M.; Mukherjee, S. S.; Zanni, M. T. Residue-specific structural kinetics of proteins through the union of isotope labeling, mid-IR pulse shaping, and coherent 2D IR spectroscopy. *Methods* **2010**, *52* (1), 12−22.
(71) Tyagi, P.; Saari, J. I.; Walsh, B.; Kabir, A.; Crozatier, V.; Forget, N.; Kambhampati, P. Two-Color Two-Dimensional Electronic Spectroscopy Using Dual Acousto-Optic Pulse Shapers for Complete Amplitude, Phase, and Polarization Control of Femtosecond Laser Pulses. *J. Phys. Chem. A* **2013**, *117* (29), 6264−6269.
(72) Fuller, F. D.; Wilcox, D. E.; Ogilvie, J. P. Pulse shaping based two-dimensional electronic spectroscopy in a background free geometry. *Opt. Express* **2014**, *22* (1), 1018−1027.
(73) de la Paz, J. A.; Bonvalet, A.; Joffre, M. Frequency-domain two-dimensional infrared spectroscopy using an acousto-optic programmable dispersive filter. *Opt. Express* **2019**, *27* (4), 4140−4146.
(74) Helbing, J.; Hamm, P. Compact implementation of Fourier transform two-dimensional IR spectroscopy without phase ambiguity. *J. Opt. Soc. Am. B* **2011**, *28* (1), 171−178.
(75) Zhang, T.; Huangfu, Z.-C.; Qian, Y.; Lu, Z.; Gao, H.; Rao, Y. Spectral Phase Measurements of Heterodyne Detection in Interfacial Broadband Electronic Spectroscopy. *J. Phys. Chem. C* **2022**, *126* (5), 2823−2832.
(76) Deng, G. H.; Wei, Q.; Qian, Y.; Zhang, T.; Leng, X.; Rao, Y. Development of interface-/surface-specific two-dimensional electronic spectroscopy. *Rev. Sci. Instrum.* **2021**, *92* (2), 023104.
(77) Li, Y.; Yang, S.; Sun, C.; Wang, L.; Wang, Q. Aqueous photofate of crystal violet under simulated and natural solar irradiation: Kinetics, products, and pathways. *Water Res.* **2016**, *88*, 173−183.
(78) Lueck, H. B.; Daniel, D. C.; McHale, J. L. Resonance Raman study of solvent effects on a series of triarylmethane dyes. *J. Raman Spectrosc.* **1993**, *24* (6), 363−370.
(79) Wu, E. C.; Ge, Q.; Arsenault, E. A.; Lewis, N. H. C.; Gruenke, N. L.; Head-Gordon, M. J.; Fleming, G. R. Two-dimensional electronic-vibrational spectroscopic study of conical intersection dynamics: an experimental and electronic structure study. *Phys. Chem. Chem. Phys.* **2019**, *21* (26), 14153−14163.

NOTE ADDED AFTER ASAP PUBLICATION

This paper was published ASAP on April 25, 2023. Additional changes were made on page three of the document, and the corrected version was reposted on May 15, 2023.

https://doi.org/10.1021/acsphyschemau.3c00011
ACS Phys. Chem Au 2023, 3, 374−385